



Irreversibility Line and Enhancement of Magnetic Flux Pinning in Sm-Doped Y123 Superconductor with CuO Nanoparticles

Raheleh Hajilou¹ · Hassan Sedghi Gamchi¹

Received: 13 August 2019 / Accepted: 15 October 2019 / Published online: 1 November 2019
© Springer Science+Business Media, LLC, part of Springer Nature 2019

Abstract

$Y_{1-x}Sm_xBa_2Cu_3O_{7-\delta}$ ($x=0.00, 0.01, 0.02$ and 0.05 wt.%) samples with Nano-CuO have been prepared by the solid-state reaction method. The effects of Sm doped in the YBCO system with Nano-CuO (40 nm) on structural, critical temperature (T_c), irreversibility line (IL), critical current density, J_c and flux line pinning force are investigated. We also measured magnetization as a function of temperature (M–T) and magnetic loops (M–H) at constant temperatures of 10, 20, 30, 40, 50 and 60 K up to 10 kG. XRD measurements show that all the sintered samples have orthorhombic structure. The sample with $x=0.01$ wt.% Sm substituted for Y on YBCO superconductor improves the critical temperature more than that of the pure Y123 and the other samples. For this sample, the zero field-cooled and field-cooled magnetization as a function of temperature measurements reveals the shift of IL to higher temperatures and magnetic fields. The critical current density and flux pinning force calculated using the Bean's critical state model indicate an enhancement of J_c and F_p for the Sm-doped $x=0.01$ sample compared with the sample with $x=0.02$ and even the pure Y123.

Keywords High- T_c superconductors · Scanning electron microscopy · X-ray scattering · Irreversibility line · Critical current density

1 Introduction

One of the interesting features of the High- T_c superconductors is the existence of an irreversibility line (IL) in the H–T plane which separates the region at lower temperatures, where the magnetic response of the vortex lattice is irreversible, from the high-temperature region, where the magnetization is reversible. This

✉ Raheleh Hajilou
rahil.hajilou@yahoo.com

¹ Department of Physics, Superconductivity Research Center, Faculty of Science, Urmia University, Urmia, Iran

behavior was observed for the first time in 1987 by Müller et al. [1] in ceramic LaBaCuO. Using zero field-cooled (ZFC) and field-cooled (FC) dc magnetization measurements in a constant field, they showed that the two curves coincided in the region between T_c and a certain lower temperature T_{irr} . This behavior has already been observed in polycrystalline samples [2, 3], single crystals [4] and thin films [5] of the Y-based superconductor as well as in the other high- T_c oxides such as the Bi-based [6, 7], Tl-based [8, 9] and even conventional superconductors [10, 11]. Considering the effects of the pinning forces and thermal fluctuations on the movement or deformation of the vortex lattice system in HTSC's which under particular conditions can involve flux creep, flux flow, thermally activated flux flow, flux lattice melting or vortex glass melting regime, many different techniques have been developed to define and measure the irreversibility line (IL). These methods are generally based on the magnetic, electrical, optical and mechanical properties of these materials. The most commonly used techniques to measure the IL or the so-called depinning line are as follows:

1. The broadening of the resistive transition $\rho(T, H)$ curves in a magnetic field: In this method, the intersection point of the two zero field-cooled (ZFC) and field-cooled (FC) resistivity $\rho(T)$ curves in a constant applied dc magnetic field, H is defined as an irreversibility temperature $T_{irr}(H)$. A noteworthy point regarding these two curves is that at temperatures lower than T_c , the ZFC curve shows a larger resistance than the FC curves and therefore moves to lower temperatures [12].
2. From the voltage–current (I – V) curves, the temperature $T_g(H)$ at which the I – V curves changes from the positive curvature at high temperatures to the negative curvature at low temperatures has been defined as the T_{irr} [13].
3. The field-cooled and zero field-cooled magnetization in a constant field, H determines the intersection temperature of these two curves as T_{irr} , below which magnetization is irreversible and above which it is reversible up to the normal state [2, 14].
4. The isothermal dc magnetization is also used to measure the IL. As the width of the hysteresis $\Delta M(H)$ is negligible near $H_{c2}(T)$ in HTSC's and that the magnetization curve in that region gives an equilibrium response, this method has been used to determine $H_{irr}(T)$ values [15].
5. The complex ac susceptibility has been widely used to measure IL, in HTSC's where the position of the inter-granular loss peak of the out-of-phase $\chi''(T)$ component, either as a function of a static field with $H_{dc} \gg H_{ac}$ at a constant dynamic field or in $H_{dc} = 0$ at various ac field amplitudes, is defined as the IL [16–18].
6. The existence of a reversible magnetization response close to $T_c(H)$ should give rise to a paramagnetic signal when the real part of the ac susceptibility is measured in a constant static field. This phenomenon, which is referred to as the differential paramagnetic effect (DPE), is used as a technique to measure the IL in High- T_c superconductor [19, 20]. In order to monitor the IL, several other procedures have also been introduced.

7. AC screening efficiency is another method which is frequently used to measure the IL in High- T_c materials [21, 22]. In this method, the sample is located between the driving and detection coils and the measured mutual inductance, with an ac field as a function of temperature under a static magnetic field that can be shown as a complex transmittivity $t = T' + iT'' = (M - M_s)(M_n - M_s)$, where M_s and M_n are the mutual inductances in the superconducting and normal states, respectively. The divergent point at T_{irr} (H) of the two ZFC and FC curves, which indeed separates the irreversible and reversible regions, is defined as the IL. This line was initially interpreted by Hebard et al. [23] as the ‘pair breaking line.’

Many efforts have been devolved to study the IL and the effect of different pinning centers on the remarkable flux pinning–depinning phenomenon. Motivated by the conflicting results reported in the literature for the effect of the introduction of defects on the IL, we have investigated superconducting properties and the IL for the Sm-substituted $Y_{1-x}Sm_xBa_2Cu_3O_{7-\delta}$ composites with $x = 0.0, 0.01, 0.02$ and 0.05 .

2 Experimental Details

The samples under study were prepared using the well-known and documented solid-state reaction technique. High-purity powders of Y_2O_3 (99.9%, Merck), Sm_2O_3 (99.9%, Merck), $BaCO_3$ (99.9%, Merck) and Nano-copper oxide (CuO 99% APS: 40 nm) were weighted in the appropriate amounts to give nominal composition of $Y_{1-x}Sm_xBa_2Cu_3O_{7-\delta}$ with $x = 0.00, 0.01, 0.02$ and 0.05 . The appropriate amount of the powders was ground thoroughly by hand using an agate mortar and pestle for 45 min. The thoroughly mixed powders were then pelletized by pressing into a 30-mm-diameter steel die (carver 4387. 4SD0B00) under 50 MPa pressure. The pellets were then quickly loaded onto an alumina tile and placed into a furnace where they were subjected to a heat treatment. The samples in the furnace were heated to 720 °C at the rate of 120 °C/h and were heated at 720 °C for 12 h followed by heating to 930 °C at the rate of 120 °C/h and were annealed at 930 °C for 12 h. Finally, the samples were furnace cooled to room temperature. After this first sintering process, all the samples had a dark color. In this sintering process, none of the products were of good quality samples. They could be easily separated into several layers. Therefore, in order to make quality and fully oxygenated samples, the sintering process was repeated. In the second cycle of the heating process, the samples were re-ground and pressed into pellets with a 30-mm diameter and with an approximate thickness of 2.2 mm under 90 MPa pressure. Pellets were then placed into a furnace and heated 930 °C at the rate of 90 °C/h. They were left to react at this temperature for 24 h. Finally, the temperature was decreased to 720 °C at a rate of 20 °C/h and then cooled to room temperature in flowing oxygen with a cooling rate of 10 °C/h. Low cooling rate in flowing oxygen was used in order to improve oxygen uptake in the samples. Unlike the first processing cycle, the products of the second cycle were uniform and almost without any cracks. X-ray diffraction measurements were taken in the range of $2\theta = 5^\circ - 60^\circ$ with CuK_α radiation source ($\lambda = 1.5406 \text{ \AA}$). Using x-pert

pro Philips analytical diffractometer, the XRD results were used in the powder diffraction programmer in order to determine a , b , c lattice parameters of the samples. The grain morphology of the surface of the samples was analyzed by scanning electron microscopy (SEM). Electrical resistivity measurements were taken as a function of temperature for the bar-shaped samples by using the standard four-point probe method with an ac lock-in technique over the temperature range of 20 K to 100 K. A constant current of 4 mA was introduced between the contacts prepared by using the silver paste. DC magnetization measurements both temperature dependence, M – T , and isothermal hysteresis loops, M – H curves, were performed using cryogenic design physical properties measurement system (ppms) model 3045, up to 60 kG using the so-called vsm option. The critical current density, J_c , was calculated using the Bean model for pure and Sm-doped $x=0.01$ samples at 10–60 K up to 60 kG applied magnetic field. The pinning force, F_p , depending on applied magnetic field and temperature was calculated from isothermal M – H measurements.

3 Result and Discussions

3.1 XRD Results

An X-ray diffraction study of the high- T_c superconductors provides information about:

1. The lattice parameters of the system,
2. The crystal structure of the material,
3. Determination of the impurities in the system and identification of the other crystalline phases in the structure of a desired system, and the oxygen contents of the material, which, in turn, controls the superconducting properties of the system.

X-ray diffraction patterns (XRD) at room temperature for our pure and Sm-substituted $Y_{1-x}Sm_xBa_2Cu_3O_{7-\delta}$ samples are illustrated in Fig. 1. It can be seen from the XRD patterns of the pure Y_{123} and the alloyed samples that all the high-intensity peaks in the XRD patterns are assigned to Y_{123} phase, indicating that the orthorhombic superconducting phase of YBCO compound has not been affected by Sm-doped atoms. There are also a few low-intensity peaks which belong to the unheated materials and green insulating phase (Y_{211}), which is commonly one of the impurities between the Y_{123} grains. The crystal symmetry of the samples was determined as orthorhombic. The oxygen content of the samples was determined by the Wolf's method, $7-\delta=76.4-5.95 C$ (Å) using the numerical relationship between δ and the c -axis lattice parameter of the sample [24]. It is well known that both the a and b lattice parameters in YBCO system have a nonlinear relationship in the orthorhombic phase, while the c -axis lattice parameter and unit cell volume show a generally linear behavior as a function of oxygen content. The higher the oxygen content of sample, the lower the c -axis lattice parameter [25]. The calculated unit cell parameters of the pure and the Sm-substituted samples,

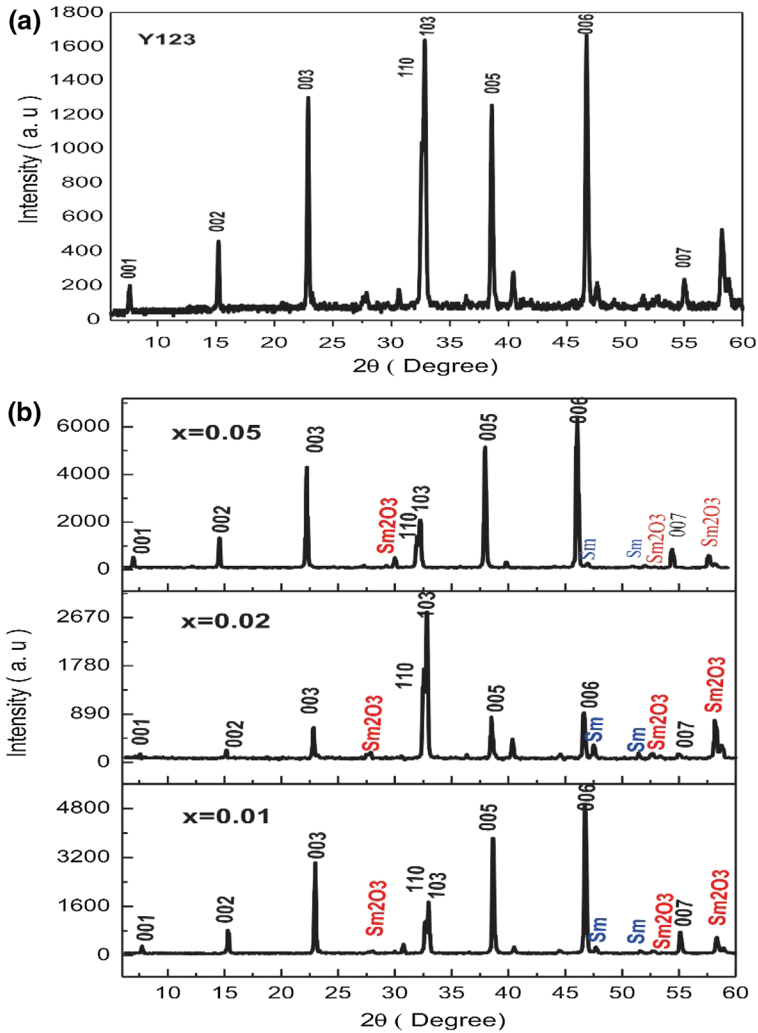


Fig. 1 **a** and **b** XRD patterns of $Y_{1-x}Sm_xBa_2Cu_3O_{7-\sigma}$ samples with $x=0.0, 0.01, 0.02$ and 0.05 (Color figure online)

orthorhombic strains, $\Delta = (b-a)/(b+a)$ and transition temperature of the samples are listed in Table 1. A quick glance at the table shows that despite very little changes in ‘a,’ ‘b’ and ‘c’ lattice parameters, the unit cell parameters of the alloyed samples are very close to the Y₁₂₃ sample, and a small decrease in c-axis length shows a slight increase in the oxygen content in the sample with $x=0.01$. The decrease in c-axis parameter is probably related to the difference in the (007) reflection in XRD patterns of this sample. The difference in the unit cell parameters can be due to occupation of the Sm ions to interstitial sites [26].

Table 1 Characteristic temperatures, lattice parameters and orthorhombicity parameters for all the $Y_{1-x}Sm_xBa_2Cu_3O_{7-\delta}$ samples

Sm content x (wt.%)	$T_{c, \text{onset}}$ (K)	$T_{c,0}$ (K)	ΔT_c (K)	a (Å)	b (Å)	c (Å)	$\Delta = (b - a)/(b + a)$	O-content
0.0	90.5	85	5.5	3.82	3.88	11.68	0.007792	6.90
0.01	93.7	88.9	4.8	3.8069	3.8895	11.666	0.009973	6.98
0.02	88.9	83.1	5.7	3.8207	3.8863	11.7059	0.008512	6.915
0.05	86.7	78.6	8.1	3.8263	3.8813	11.7113	0.007136	6.848

3.2 SEM Measurements

Since the discovery of High- T_c superconductors, microstructural studies of the materials have played a crucial role in the understanding of these materials. Especially, the investigation of grain boundaries and second phases in the copper oxide superconductors has been carried out successfully by using high-resolution scanning electron microscopy (SEM). Typical electron micrographs of the $Y_{1-x}Sm_xBa_2Cu_3O_{7-\delta}$ composites are shown in Fig. 2. It is well known that in high- T_c superconductors, the formation and size of the superconducting grains and deliberately introduced impurities play an important role in electrical conductivity and magnetic properties of the system both in the normal and superconducting states [27]. The light areas in SEM micrographs indicate the superconducting metallic regions, while the dark areas correspond to the inter-granular material. It was found that the two samples ($x=0.01, 0.02$) have a uniform appearance with less porosity and larger grain size, crystallization and better inter-granular bonding. As it can be seen from the figures, the grains in the pure Y123 sample are almost circular with small grain size, while in the composite samples obviously in Sm-doped $x=0.01$ sample rod-like elongated grains have been found. In this sample compared to the pure Y123 and other Sm-doped samples, grain boundary area is dropped, which is responsible for the high transport critical current density and flux pinning force in the YBCO superconductor. Clearly, it is obvious from the figures that existence of Sm in fractions does not react with YBCO to form a new phase or structure as was observed in XRD patterns. With an increase in Sm in the dopant samples, grain size and inter-granular interactions have decreased, and the porosity of the samples starts to increase.

3.3 Electrical Resistivity

For measurement of electrical resistivity as a function of temperature ($\rho-T$), bar-shaped specimens were cut from each sintered pellet of the composite samples. The dimensions of the samples were typically $4 \times 1.5 \times 6 \text{ mm}^3$. Electrical resistivity was measured using the standard four-point probe method with an ac lock-in technique over the temperature range of 20 K to 100 K. Figure 3 a, b shows the resistivity as a function of temperature along with its temperature derivative for the $Y_{1-x}Sm_xBa_2Cu_3O_{7-\delta}$ samples. From Fig. 3a, it can be seen that the

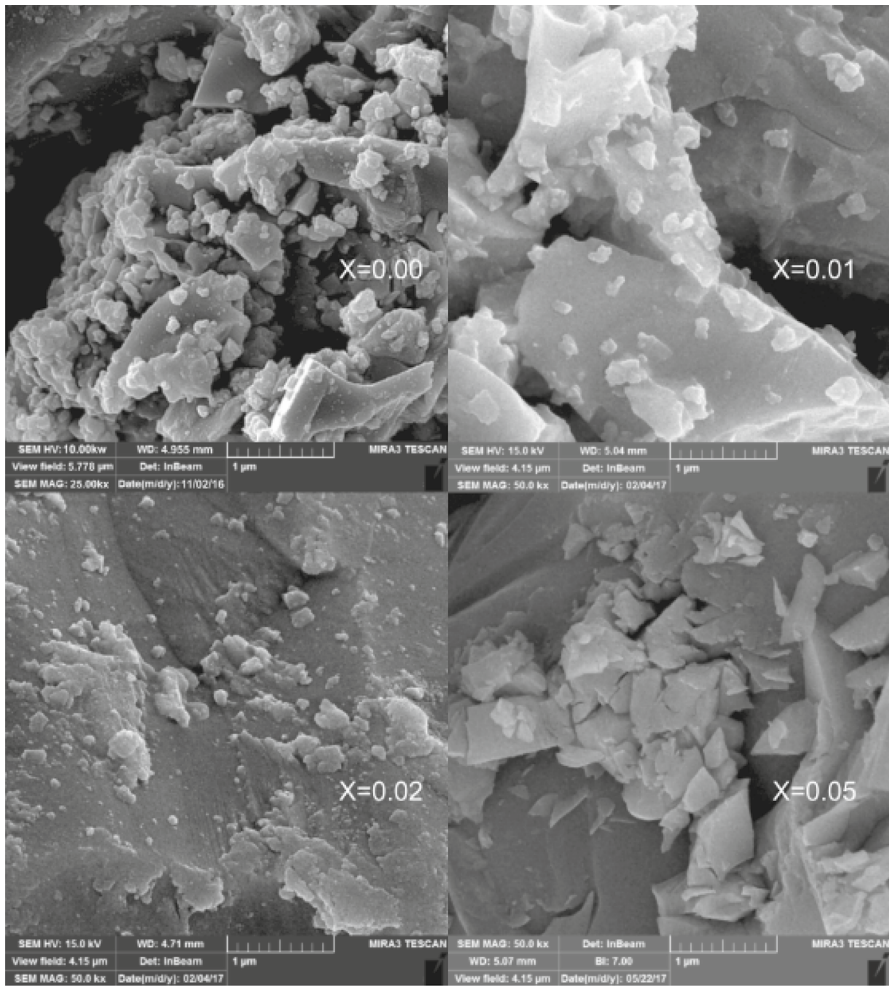


Fig. 2 SEM microphotographs of the $Y_{1-x}Sm_xBa_2Cu_3O_{7-d}$ with $x=0.0, 0.01, 0.02$ and 0.05

resistivity decreases almost linearly at normal state, showing a clear metallic behavior for all the samples. The normal state resistivity starts to increase with further Sm content samples. Figure 3b shows that the superconductivity state of all the samples shows a single-step drop to the transition temperature, except for $x=0.05$ wt % sample which shows a two-step drop to T_C , which is clear in the appearance of two humps in the temperature derivative plot of the sample. However, the other measured samples show a single-step drop to the superconducting state which is clear in Fig. 3b. These figures show that the superconducting transition temperature is sensitive to the concentration of Sm. This behavior has been observed by other research groups [28]. The dissipation width, ΔT , for the Sm content samples shows a broadened resistive transition to a fully

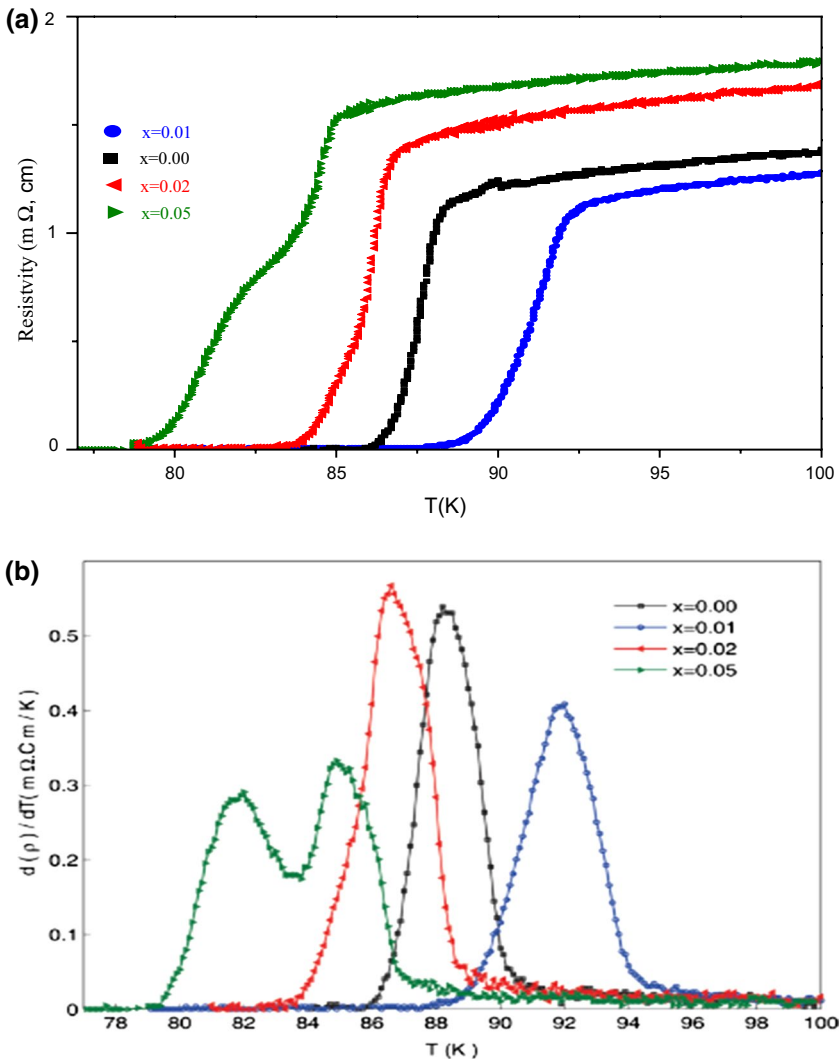


Fig. 3 **a** ($\rho - T$) curves and **b** its temperature derivative of the $Y_{1-x}Sm_xBa_2Cu_3O_{7-\delta}$ with $x=0, 0.01, 0.02$ and 0.05 (Color figure online)

superconducting state, showing the increase in the weak link between superconducting grains. It is clear from Fig. 3a that the sample with $x=0.01$ wt.% Sm content shows a transition temperature higher than all the other samples even the pure Y_{123} . These results show there is a critical concentration of Sm to improve the superconductivity in Sm-substituted samples.

3.4 Magnetic Properties

Since the sample with $x=0.01$ wt.% Sm content shows a higher T_C , than the pure and the other alloyed samples, in order to gain more information concerning the critical parameters of this sample, we especially concentrated on the positive effect of partially Sm-doped sample with $x=0.01$ and compared with the pure Y_{123} and $x=0.02$ samples. Figure 4a–c shows a typical data set of the temperature dependence of the magnetic moment (M – T) curves measured under zero field-cooled (ZFC) and field-cooled (FC) modes in magnetic fields of (a) $H=10$ kG and (b) $H=60$ kG

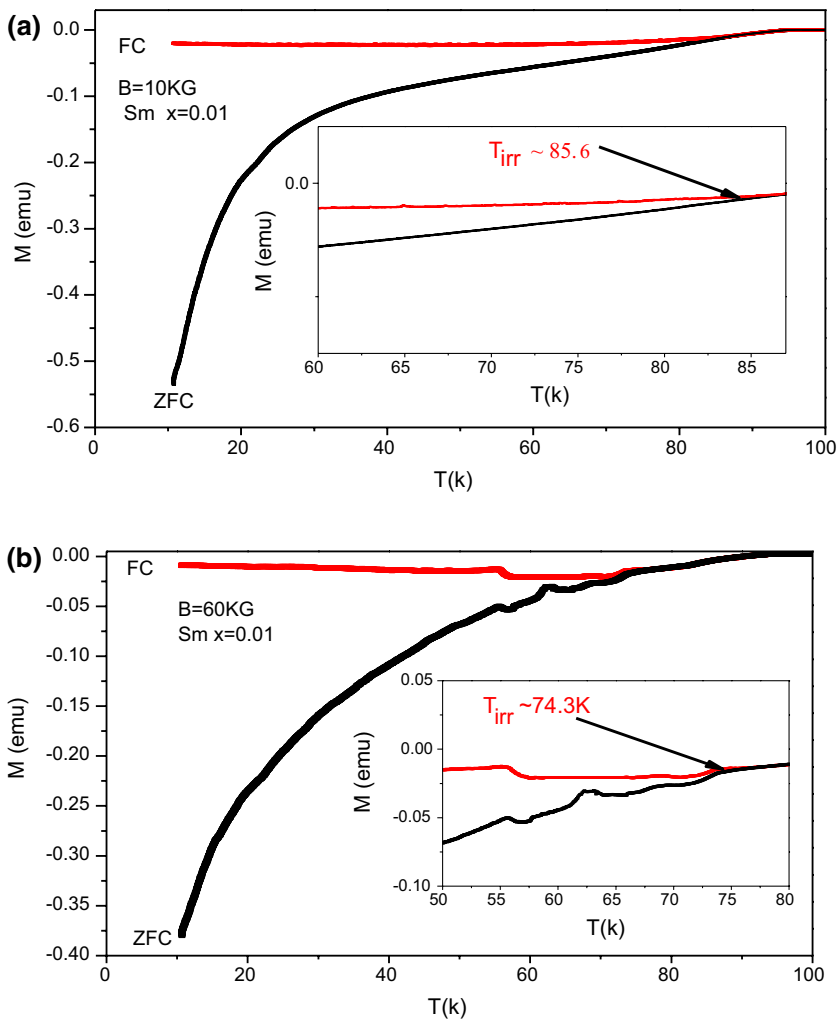


Fig. 4 Plot of ZFC and FC magnetization curves **a** for $H=10$ kG and **b** $H=60$ kG showing the irreversibility limit T_{irr} (H) for the Sm dopant $x=0.01$ sample. Insets show irreversibility temperature range in the enlarged scale (Color figure online)

for the sample of $x=0.01$. In the zero field-cooled process, the sample was first cooled in zero field from 100 K which is above the transition temperature, T_c , to the lowest desired temperature, 10 K. Then, applied dc magnetic field was selected and the magnetic response of the sample was recorded on warming the sample. In the FC process, the sample was cooled down from 100 K in the presence of the desired magnetic field and then warming in the same field while data were being recorded. The data from the magnetic response of the sample were plotted as a function of temperature. The point where the FC and ZFC curves merge together denotes the irreversibility temperature T_{irr} . This measurement was repeated for various fields to determine the IL. The insets show the temperature range which includes $T_{irr}(H)$. As is clear in Fig. 4a, b compared with the field-cooled magnetic response, M_{FC} , the zero field-cooled magnetization, M_{ZFC} , values are higher. At first glance, this result appears unusual because the FC curve corresponds to the case that there should be flux trapped in the sample and is expected to show high magnetic response than the ZFC data. However, in the superconducting glass picture [29], when the superconductor clusters are cooled slowly in a fixed dc field, the resulting configuration will be in equilibrium because the slow cooling allows the clusters to be annealed at relatively high temperatures. However, by cooling in zero field and turning on the field at a fixed low temperature, the clusters will be in a non-equilibrium state which gives rise to a metastable magnetization for the ZFC curves. In this process, the clusters have no time to equilibrate as the field is turned on. In Fig. 5a, b, we display typical data set of the temperature dependence of the magnetic moment (M - T) for the pure Y123 sample (a) at 10 kG and (b) 60 kG. As is clear from this figure, the T_{irr} for a desired magnetic field always is lower than that of the Sm-doped $x=0.01$ sample. These results clearly show that the small quantity of the Sm ($x=0.01$) not only does not negatively affect the critical properties of the Y123 system, but also acts as the pinning centers and increases the flux pinning behavior. The positive flux pinning effects of Se- and Eu-doped Y123 system also are shown by other research groups [30, 31]. Figure 6a, b shows typical data of (M - T) measurements for the Sm-doped $x=0.02$ sample. Because the solubility limits of Sm in YBCO are $x=0.01$, unlike the $x=0.01$ sample at both measuring fields T_{irr} moved to lower temperatures which shows that increasing the Sm dopant in YBCO system higher than a certain volume fraction decreases the electric and magnetic behavior of the composites as also can be seen in ρ - T curves. The T_{irr} position for all the measured samples moves to lower temperatures as the measured magnetic field is increased. The results of $T_{irr}(H)$ measurements as a function of applied magnetic field up to 60 kG are plotted in Fig. 6 for the Sm-doped $x=0.01$, 0.02 and pure Y₁₂₃ samples. As is shown in this figure, there exists a remarkable large temperature range in which flux-line motion is reversible. The onset of reversible motion of flux lines interpreted by different groups is due to melting of a crystalline flux lattice [32] or of the glass-to-liquid phase transition [33], or simply is due to the enhanced rate of thermally activated flux motion [34]. As is evident from Fig. 7, the $T_{irr}(H)$ data for all the samples show a nonlinear behavior with an almost down curvature in the H - T plane, which is characteristic of the demarcation between reversible and irreversible magnetization behaviors of HTSC's. In order to examine the scaling behavior of the T_{irr} with magnetic field in the measured samples, by taking into account the observed universal

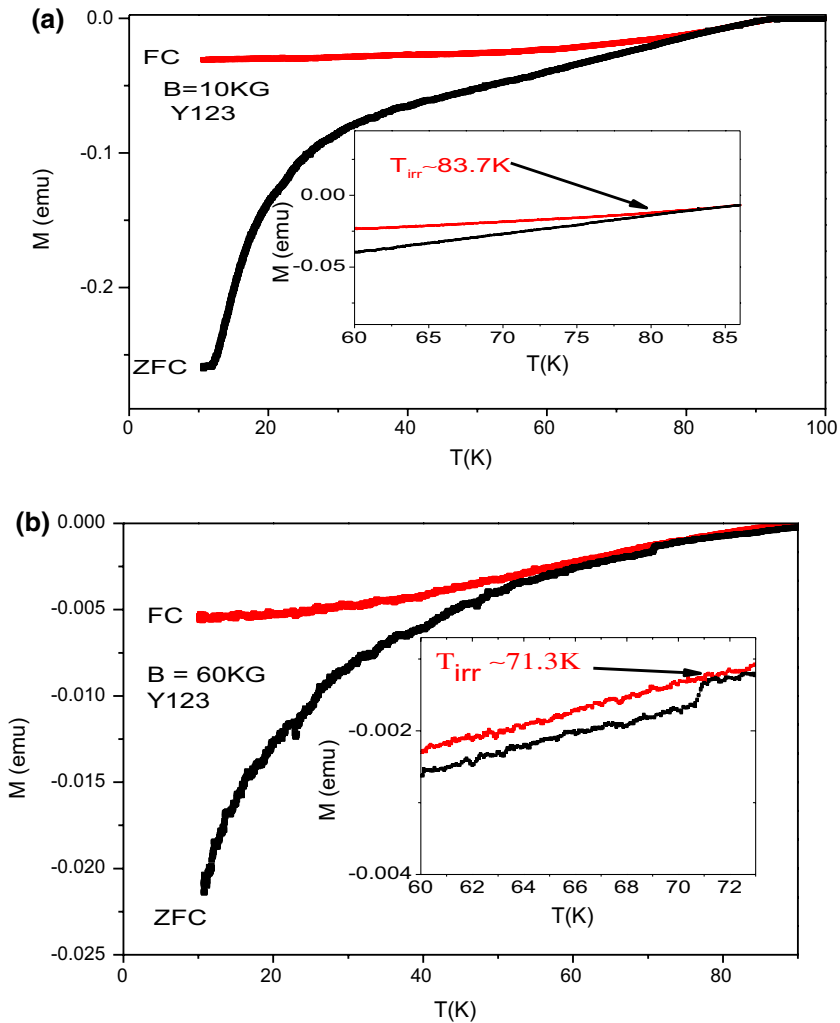


Fig. 5 Plot of ZFC and FC magnetization curves **a** for $H = 10$ kG and **b** $H = 60$ kG showing the irreversibility limit $T_{irr}(H)$ for the pure Y123 sample. Insets demonstrate: irreversibility temperature range in the enlarged scale (Color figure online)

scaling of the reduced irreversibility temperature $t = (T_{irr}/T_c)$ with the applied magnetic field strength, $H = a(1-t)^q$, we have replotted the data from Fig. 7, as $\ln(H)$ versus $\ln(1-t)$, which is shown in Fig. 8. As can be seen from this figure, the irreversibility temperature, $(1-T_{irr}/T_c)$ as a function of applied magnetic fields for all the samples, is a straight line. The irreversibility line obtained for the Sm-doped $x = 0.01$ sample is located at higher temperatures and magnetic fields than that of the $x = 0.02$ and pure Y123 samples. Within experimental accuracy, the values of the exponent q are 1.51 for the Sm-doped $x = 0.01$ and 1.61, for the pure Y123 and $x = 0.02$ samples. The pre-exponential parameter “ a ” obtained for all the samples is to be 0.97. The

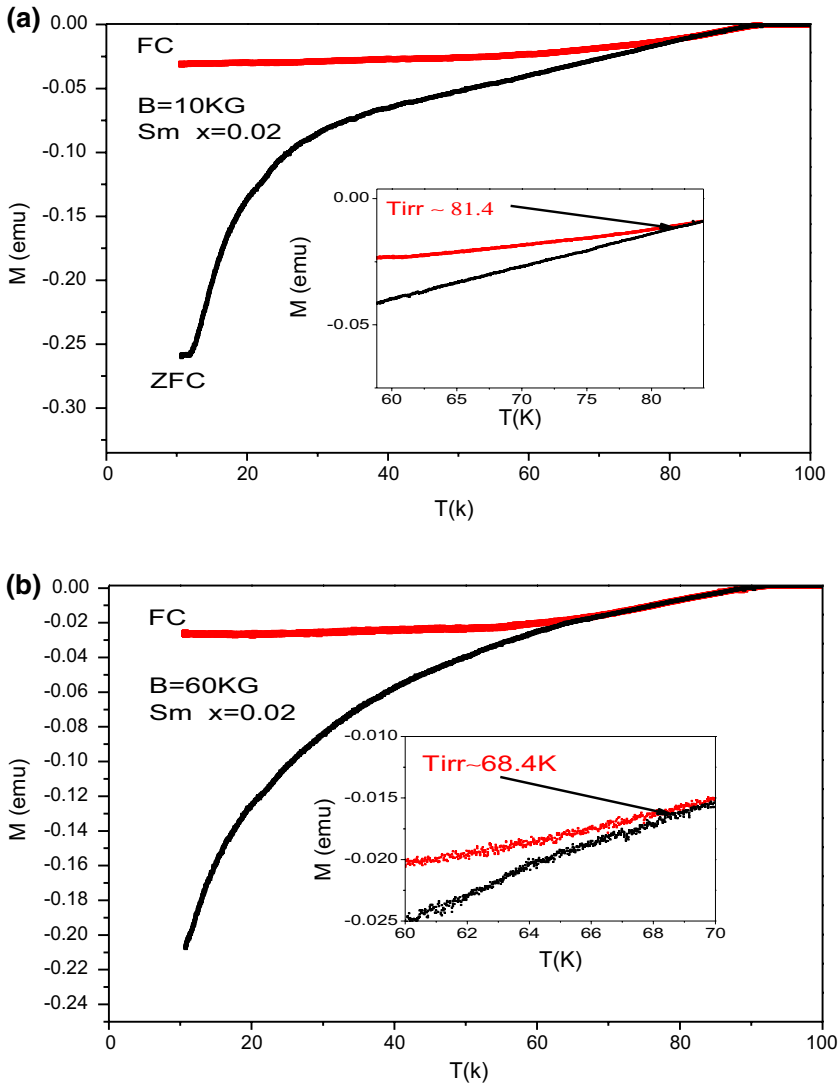


Fig. 6 Plot of ZFC and FC magnetization curves **a** for $H=10$ kG and **b** $H=60$ kG showing the irreversibility limit $T_{irr}(H)$ for the Sm dopant $x=0.02$ sample. Insets demonstrate: irreversibility temperature range in the enlarged scale (Color figure online)

form of the IL, as described by the power law relationship with $q=1.5$, has been considered theoretically in terms of a number of models. Such a law is similar to the Almeida–Thouless in spin glasses [35]. This behavior has also been predicted by models involving flux pinning and flux flow [36].

We also measured the isothermal magnetic hysteresis, M – H loops for the pure Y123 and the Sm-doped $x=0.01$, 0.02 samples. The results of this measurement at different constant temperatures 10 K, 20 K, 30 K, 40 K, 50 K and 60 K up to 10 kG are shown in

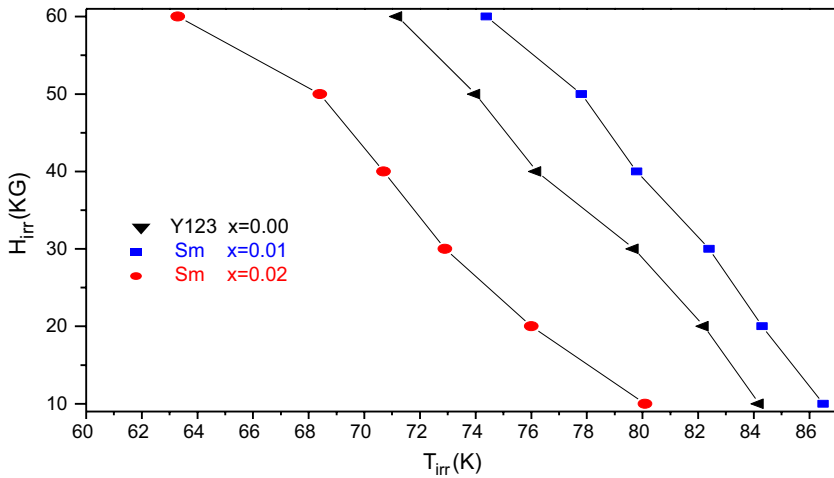


Fig. 7 Irreversibility line, T_{irr} (H), as a function of magnetic field for the Sm dopant $x=0.01$ and pure Y_{123} samples found from Figs. 4 and 5. The solid lines are guides to the eye (Color figure online)

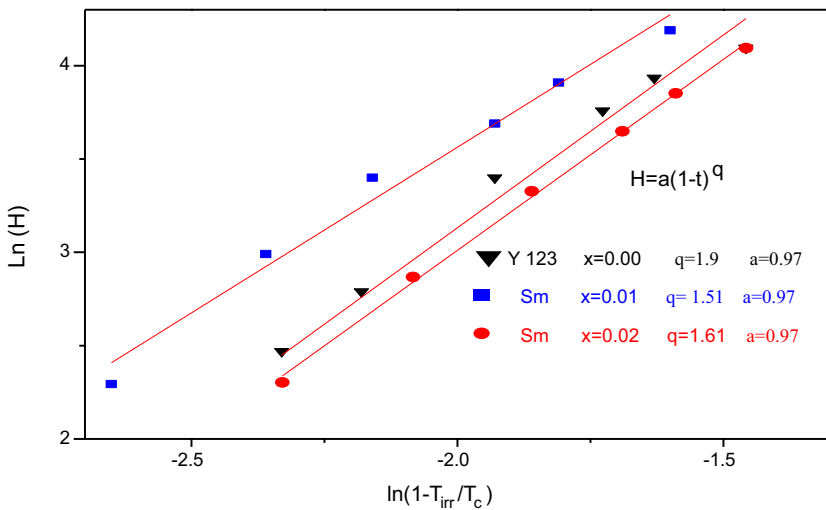


Fig. 8 $\ln(1 - T_{irr}/T_c(0))$ versus $\ln(H)$, for a pure Y_{123} , Sm-doped $x=0.01$ and 0.02 samples. The best-fit straight lines have almost the same slope for both samples (Color figure online)

Fig. 9a–c. It is clear from these figures that with an increase in measuring temperature the hysteresis loops show narrow shapes. This behavior is clearly shown in Fig. 9. The higher the pinning strength, the bigger the critical current, and hence, the wider the hysteresis loops. It is well known that the width and behavior of this hysteresis loop are characteristics of the bulk critical current density in HTSC's and its dependence on the magnetic flux density [37]. The wider the hysteresis loop is, the higher the bulk critical current density will be. The critical current density for rectangular sample was

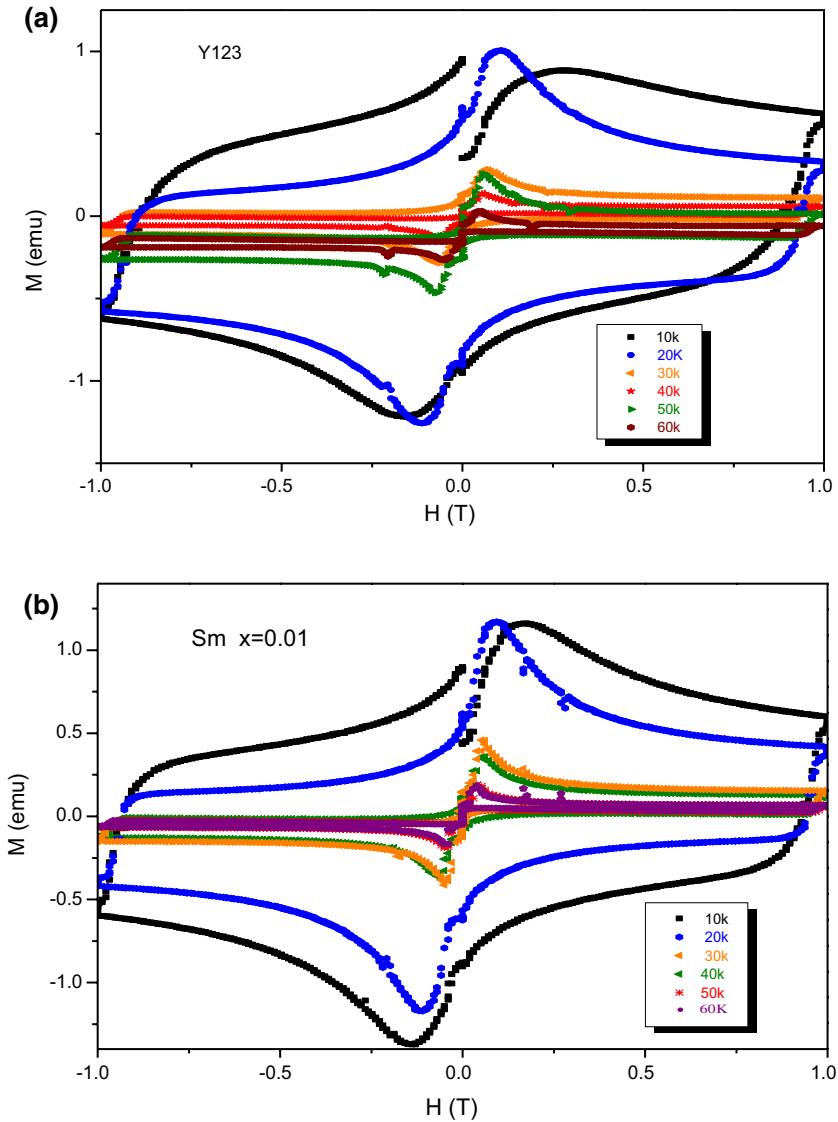


Fig. 9 Isothermal magnetization versus field curves (M - H loop) at 10 K, 20 K, 30 K, 40 K, 50 K and 60 K for the **a** the pure Y123, **b** the Sm $x=0.01$ and **c** $x=0.02$ samples (Color figure online)

calculated by using the Bean's critical state model [38] for polycrystalline superconductors given by:

$$J_C = 20 \frac{\Delta M}{a \left(1 - \frac{a}{3b}\right)} \quad (1)$$

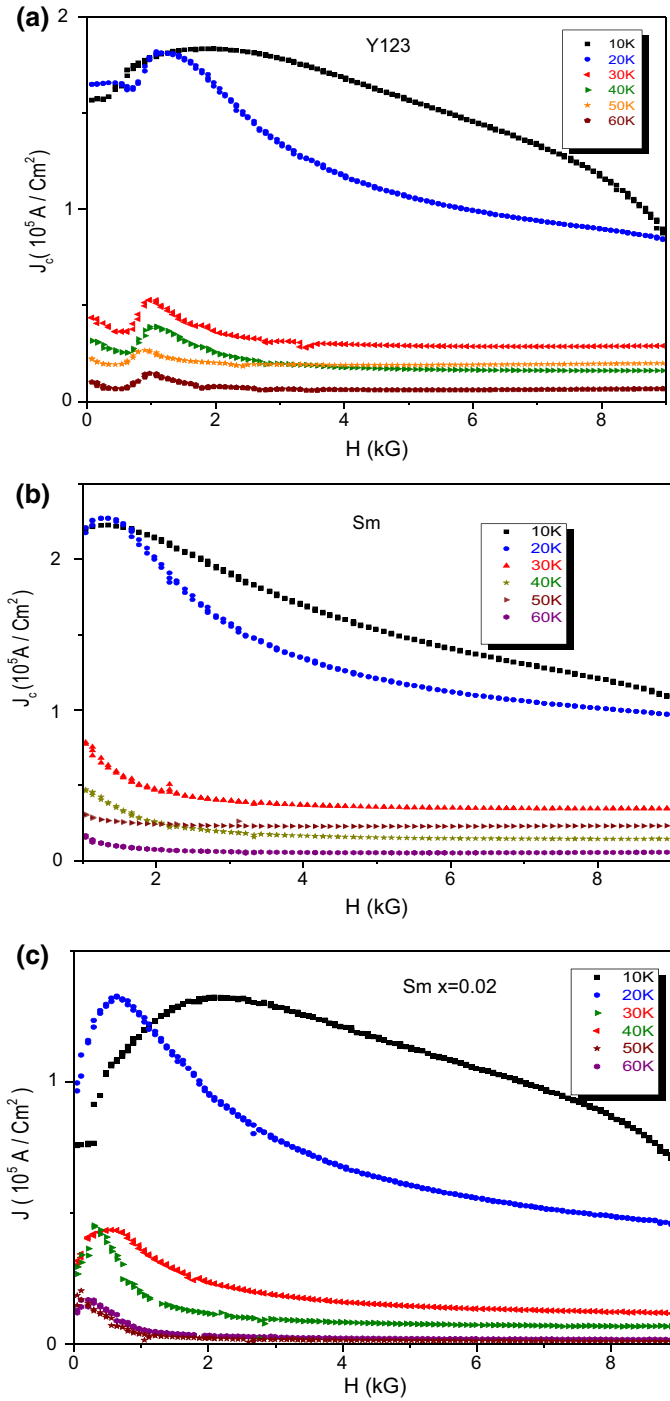


Fig. 10 Plot of J_c as a function of magnetic field for **a** the pure Y123, **b** the Sm-doped $x=0.01$ and **c** $x=0.02$ samples (Color figure online)

where $\Delta M = M^+ - M^-$ is the width of magnetization hysteresis, and a and b ($a < b$) are the dimensions of the sample. The applied magnetic field dependence of J_C (H), at 10 K, 20 K, 30 K, 40 K, 50 K and 60 K for the samples with $x=0.00$, 0.01 and 0.02, is presented in Fig. 10. The maximum J_C value was determined to be 2.28×10^5 A/cm² at 10 K for the applied magnetic field of 1 kG for the Sm-doped $x=0.01$ sample, whereas the maximum J_C value is 1.8×10^5 A/cm² at 10 K for the same applied magnetic field for the pure Y123 sample. It is clear from Fig. 10 that the J_C values decrease with an increase in the applied magnetic field and increase the constant measuring temperature for all samples. As explained in (M–T) measurement, Sm-doped sample with $x=0.01$ enhanced the pinning of the flux lines and hereby results in an enhancement of J_c .

We have calculated the magnetic field dependence of the pinning force $F_p = J_c \times B$ for the pristine Y₁₂₃ and the Sm-doped $x=0.01$, 0.02 samples. The variation in F_p as a function of the applied magnetic field at 10 K, 20 K, 30 K, 40 K, 50 K and 60 K is shown in Fig. 11a–c. This figure clearly shows that the pinning force increases with applied magnetic field at all measuring temperatures for the measured samples. The comparison of the figures (a) for the pure Y₁₂₃ and (b) for the Sm-doped $x=0.01$ samples shows that the values of the pinning force in partial doping Y₁₂₃ with Sm: $x=0.01$ are considerably higher than that of the pristine sample over the entire range of the applied magnetic field at each desired measuring temperature. In the case of a measuring temperature at 10 K for the 9 kG magnetic field, the pinning force shows nearly 1.2-fold increase with respect to the pure sample. These values of F_p are significantly higher than the values found in YBCO:Se composites fabricated at different temperatures under oxygen atmosphere [31]. It is well known that when the Lorentz force acting on the fluxoids exceeds the pinning energy, F_p , of the flux line lattice, the fluxoids begin to move across the sample and the material goes to the resistive state. As we have seen in Sect. 3.3, Sm-doped $x=0.01$ sample shows a higher transition temperature and critical current density than that of the pure Y₁₂₃ sample. The Sm atoms in Y₁₂₃ system, apart from improving the grain boundary, may act as artificial pinning centers which itself results in the enhancement of J_c and dominance of the pinning force over the Lorentz force even at high magnetic fields. Some other research groups [39–41] found a similar behavior in Y₁₂₃ system and reported that partial doping of the Y⁺³ in the Y₁₂₃ with Cu⁺² increases grain boundary J_c , which itself causes an increase in pinning force.

4 Conclusion

We have investigated the effects of Sm-substituted Y_{1-x}Sm_xBa₂Cu₃O_{7- δ} composites on the electrical and magnetic properties of YBCO high-temperature superconductor. Through XRD and SEM analysis, we found that the structure of all the samples has the Y123 orthorhombic phase. The results of ρ (T) measurements showed that Sm with $x=0.01$ wt.% has acted in an effective manner and increased the critical temperature. It also showed that the normal resistivity of the Sm-doped YBCO compound samples was increased. Besides, desired value of Sm-substituted YBCO sample with $x=0.01$ wt.% displays lower resistivity in the normal state and higher

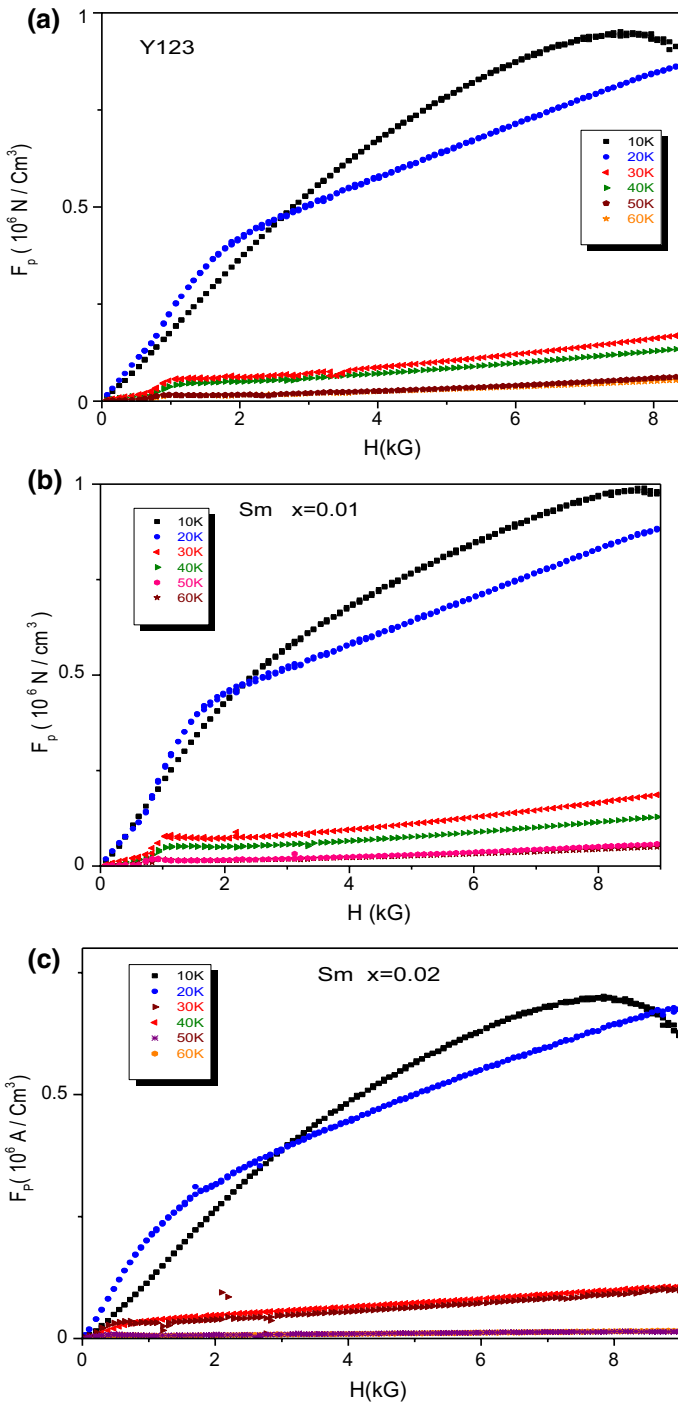


Fig. 11 F_p - H dependences at 10 K, 20 K, 30 K, 40 K, 50 K and 60 K **a** for the pure Y123 and **b** Sm-doped $x=0.01$ and $x=0.02$ samples (Color figure online)

J_c and pinning force, F_p values. So an enhancement can be beneficial in T_c and J_c of Sm-substituted YBCO compounds for the practical applications of these high-temperature superconducting materials.

References

1. J.G. Bednorz, K.A. Müller, Possible high T_c superconductivity in the Ba–La–Cu–O system. *Z. Phys. B* **64**, 189 (1986). <https://doi.org/10.1007/bf01303701>
2. Y. Xu, M. Suenaga, Y. Gao, J.E. Crow, N.D. Spencer, Irreversibility temperatures in *c*-axis-oriented powders of $\text{YBa}_2\text{Cu}_3\text{O}_7$, $\text{Bi}_2\text{Sr}_2\text{CaCu}_2\text{O}_8$, and $\text{Bi}_2\text{Sr}_2\text{Ca}_2\text{Cu}_3\text{O}_{10}$. *Phys. Rev. B* **42**, 8756 (1990). <https://doi.org/10.1103/PhysRevB.42.8756>
3. J. Vanacken, E. Osquiguil, Y.B. Ruynseraede, Irreversibility line and critical currents in oxygen deficient $\text{YBa}_2\text{Cu}_3\text{O}_x$ ceramics. *Physica C* **18**, 163 (1991). [https://doi.org/10.1016/0921-4534\(91\)90780-3](https://doi.org/10.1016/0921-4534(91)90780-3)
4. Y. Yeshurun, A.P. Malozemoff, Giant Flux Creep and Irreversibility in a Y–Ba–Cu–O Crystal: an alternative to the superconducting-glass model. *Phys. Rev. Lett.* **60**, 2202 (1988). <https://doi.org/10.1103/PhysRevLett.60.2202>
5. L. Civale, T.K. Worthington, A. Gupa, Thickness dependence of the irreversibility line in $\text{YBa}_2\text{Cu}_3\text{O}_{7-x}$ thin films. *Phys. Rev. B* **43**, 5425 (1991). <https://doi.org/10.1103/PhysRevB.43.5425>
6. W. Kritscha, F.M. Squerzopf, H.W. Weber, G.W. Grabtree, Y.C. Chang, P.Z. Jiang, Critical currents in superconductors for practical applications. *Europhys. Lett.* **12**, 17999 (1990). <https://doi.org/10.1142/3642>
7. H. Zaleski, F.S. Razavi, Irreversibility-line study in the polycrystalline $\text{Bi}_2\text{Sr}_2\text{CaCu}_2\text{O}_8$ superconductor. *Phys. Rev. B* **43**, 1423 (1991). <https://doi.org/10.1103/PhysRevB.43.1423>
8. J.S. Munoz, M. Pont, T. Puig, Z.Z. Sheng, Y. Xin, D.X. Gun, D.O. Pederson, Effect of a bias field (up to 1 T) on the a. c. susceptibility of $\text{Cr}_{0.3}\text{Tl}_1\text{Ba}_2\text{Ca}_2\text{Cu}_3\text{O}_x$. *Cryogenics* **32**, 1042 (1992). [https://doi.org/10.1016/0011-2275\(92\)90024-5](https://doi.org/10.1016/0011-2275(92)90024-5)
9. M. Pont, T. Puig, J.S. Munoz, Z.Z. Sheng, Y. Xin, D.X. Gun, D.O. Pederson, Effect of Cr and V substitution on the properties of bulk Tl-based superconductors. *Cryogenics* **33**, 91 (1993). [https://doi.org/10.1016/0011-2275\(93\)90083-Z](https://doi.org/10.1016/0011-2275(93)90083-Z)
10. M. Suenaga, A.K. Ghosh, Y. Xu, D.O. Welsh, Irreversibility temperatures of Nb_3Sn and Nb-Ti . *Phys. Rev. Lett.* **66**, 1777 (1991). <https://doi.org/10.1103/PhysRevLett.66.1777>
11. A.K. Grover, R. Kumar, S.K. Malik, P. Chaddah, V. Sankaranara Yahan, C.K. Subramanian, Quasi-irreversibility temperature in a type-I superconductor. *Phys. Rev. B* **43**, 6151 (1991). <https://doi.org/10.1103/PhysRevB.43.6151>
12. J.F. Carolan, W.N. Hardy, R. Krahn, J.H. Brewer, R.C. Thompon, A.C.D. Chaklader, The superconducting glass transition in $\text{YBa}_2\text{Cu}_3\text{O}_{7-\sigma}$. *Solid State Commun.* **64**, 717–719 (1987). [https://doi.org/10.1016/0038-1098\(87\)90686-7](https://doi.org/10.1016/0038-1098(87)90686-7)
13. R.H. Koch, V. Foghietti, W.J. Gallagher, G. Koren, A. Gupla, M.P.A. Fisher, Experimental evidence for vortex-glass superconductivity in Y–Ba–Cu–O. *Phys. Rev. Lett.* **63**, 1511 (1989). <https://doi.org/10.1103/PhysRevLett.63.1511>
14. Y. Xu, M. Suenaga, Irreversibility temperatures in superconducting oxides: the flux-line-lattice melting, the glass-liquid transition, or the depinning temperatures. *Phys. Rev. B* **43**, 5516 (1991). <https://doi.org/10.1103/PhysRevB.43.5516>
15. D.K. Finnemore, R.N. Shelton, J.R. Clem, R.W. McCallum, H.C. Ku, R.E. McCarly, S.C. Chen, P.K. Lavins, V. Kogan, Magnetization of superconducting lanthanum copper oxides. *Phys. Rev. B* **35**, 5319 (1987). <https://doi.org/10.1103/PhysRevB.35.5319>
16. A.P. Malozemoff, T.K. Worthington, Y. Yeshurun, F. Holtzberg, Frequency dependence of the ac susceptibility in a Y–Ba–Cu–O crystal: a reinterpretation of H_{c2} . *Phys. Rev. B* **37**, 7203 (1988). <https://doi.org/10.1103/PhysRevB.38.7203>
17. C.H. Heinzl, C.H. Neumann, P. Ziemann, Anisotropy of the irreversible magnetic behaviour of YBaCuO and TlBaCaCuO single crystals: a comparative a.c.-susceptibility study. *Euro Phys. Lett.* **13**, 531 (1990). <https://doi.org/10.1209/0295-5075/13/6/010>

18. V. Skumryev, M.R. Koblishka, H. Kronmüller, Sample size dependence of the AC-susceptibility of sintered $\text{YBa}_2\text{Cu}_3\text{O}_{7-\sigma}$ superconductors. *Physica C* **184**, 332 (1991). [https://doi.org/10.1016/0921-4534\(91\)90399-J](https://doi.org/10.1016/0921-4534(91)90399-J)
19. S. Ramakrishnan, R. Kumar, P.L. Pavlose, A.K. Grover, P. Chaddah, Comparison of various methods to determine experimentally the irreversibility line in superconductors. *Phys. Rev. B* **44**, 9514 (1991). <https://doi.org/10.1103/PhysRevB.44.9514>
20. A.F. Khoder, M. Couach, J.L. Jorda, Flux density in the mixed state in the high- T_c superconductors and the predictions of Abrikosov theory. *Phys. Rev. B* **42**, 8714 (1990). <https://doi.org/10.1103/PhysRevB.42.8714>
21. E.R. Yacoby, A. Shaulov, Y. Yeshurum, M. Konczykowski, F. Rulleir Albenque, Irreversibility line in $\text{YBa}_2\text{Cu}_3\text{O}_7$ samples A comparison between experimental techniques and effect of electron irradiation. *Physica C* **199**, 15 (1992). [https://doi.org/10.1016/0921-4534\(92\)90534-J](https://doi.org/10.1016/0921-4534(92)90534-J)
22. J. Gilchrist, M. Konczykowski, AC screening measurement for the characterization of oxide superconductors, I. Application to ceramics. *Physica C* **168**, 123 (1990). [https://doi.org/10.1016/0921-4534\(90\)90114-T](https://doi.org/10.1016/0921-4534(90)90114-T)
23. A.F. Hebard, P.L. Gammel, C.E. Rice, A.F.J. Levi, Pair-breaking description of the vortex-depinning critical field in $\text{YBa}_2\text{Cu}_3\text{O}_7$ thin. *Phys. Rev. B* **40**, 5243 (1989). <https://doi.org/10.1103/PhysRevB.40.5243>
24. T. Wolf, I. Apfelstedt, W. Goldcker, H. Küpfer, R. Flükiger, Preparation and characterization of isotropic and textured $\text{YBa}_2\text{Cu}_3\text{O}_{7-x}$ with high density and low residual resistivity. *Physica C* **351**, 153–155 (1988). [https://doi.org/10.1016/0921-4534\(88\)90628-4](https://doi.org/10.1016/0921-4534(88)90628-4)
25. R.M. Hazen, L.W. Finger, R.J. Angel, C.T. Perwitt, N.L. Ross, H.K. Mao, C.G. Hadjidakos, P.H. Hor, R.L. Meng, C.W. Chu, Crystallographic description of phases in the Y–Ba–Cu–O superconductor. *Phys. Rev.* **335**, 7238 (1987). <https://doi.org/10.1103/PhysRevB.35.7238>
26. M.B. Turkoz, S. Nezir, C. Terzioglu, A. Varilci, G. Yildirim, Investigation of Lu effect on $\text{YBa}_2\text{Cu}_3\text{O}_{7-\sigma}$ superconducting, compounds. *J. Mater. Sci.: Mater. Electron.* **24**, 896–905 (2013). <https://doi.org/10.1007/s10854-012-0846-y>
27. B. Abeles, H.L. Pinch, J.I. Gittleman, Percolation conductivity in W-a1203 granular metal films. *Phys. Rev. Lett.* **35**, 247 (1975). <https://doi.org/10.1103/PhysRevLett.35.247>
28. S.P.K. Naik, P.M.S. Raju, V. Seshubai, Role of Sm and Nb on the preform optimized infiltration growth processed YBCO superconductors. *Mater. Chem. Phys.* **182**, 503–507 (2016). <https://doi.org/10.1016/j.matchemphys.2016.07.064>
29. K.A. Müller, M. Takashige, J.G. Bednorz, Flux trapping and superconductive glass state in $\text{La}_2\text{CuO}_{4-y}$: Ba. *Phys. Rev. Lett.* **58**, 1143 (1987). <https://doi.org/10.1103/PhysRevLett.58.1143>
30. M. Cai, M.H. Fang, X.J. Zhang, Z.K. Jiao, Q.R. Zhang, X.S. Rong, B.R. Zhao, Investigations on flux creep and $J_c(T, B)$ behavior in $\text{Y}_{1-x}\text{Eu}_x\text{Ba}_2\text{Cu}_3\text{O}_{7-\sigma}$. *Phys. State. Sol. (a)* **147**, 221 (1995). <https://doi.org/10.1002/pssa.2211470123>
31. Z.D. Yakinci, D.M. Gokhfed, E. Altin, F. Kurt, S. Altin, D. Demirel, M.A. Aksan, M.E. Yakinci, Jc enhancement and flux pinning of Se substituted YBCO compound. *J. Mater. Sci.* **24**, 4790 (2013). <https://doi.org/10.1007/s10854-013-1476-8>
32. P.L. Gammel, L.F. Schneemeyer, J.V. Waszczak, D.J. Bishop, Evidence from mechanical measurements for flux-lattice melting in single-crystal $\text{YBa}_2\text{Cu}_3\text{O}_7$ and $\text{Bi}_{2.2}\text{Sr}_2\text{Ca}_{0.8}\text{Cu}_2\text{O}_8$. *Phys. Rev. Lett.* **61**, 1661 (1988). <https://doi.org/10.1103/PhysRevLett.61.1666>
33. D.S. Fisher, M.P.A. Fisher, D.A. Huse, Thermal fluctuations, quenched disorder, phase transitions, and transport in type-II superconductors. *Phys. Rev. B* **43**, 130 (1991). <https://doi.org/10.1103/PhysRevB.43.130>
34. P. Esquinazi, A. Gupta, H.F. Braun, The depinning line of a Y (Gd) $\text{Ba}_2\text{Cu}_3\text{O}_x$ single crystal. *Phys. B* **165**, 1151 (1990). [https://doi.org/10.1016/S0921-4526\(09\)80161-0](https://doi.org/10.1016/S0921-4526(09)80161-0)
35. J.R.L. de Almeida, D.J. Thouless, Stability of the Sherrington-Kirkpatrick solution of a spin glass model. *J. Phys. A* **11**, 983 (1978). <https://doi.org/10.1088/0305-4470/11/5/028>
36. M. Tinkham, resistive transition of high-temperature superconductors. *Phys. Rev. Lett.* **61**, 1658 (1988). <https://doi.org/10.1103/PhysRevLett.61.1658>
37. A. Öztürka, İ. Düzgünb, S. Çlebi, The effect of partial Lu doping on magnetic behaviour of YBCO (123) superconductors. *J. Alloys Compd.* **495**, 104–107 (2010). <https://doi.org/10.1016/j.jallcom.2010.01.095>
38. C.P. Bean, Magnetization of hard superconductors. *Phys. Rev. Lett.* **8**, 250–253 (1962). <https://doi.org/10.1103/PhysRevLett.8.250>

39. A. Schmehl, B. Goetz, R.R. Schuls, C.W. Schneider, H. Bielefeldt, H. Hilgenkamp, J. Mannhart, Doping-induced enhancement of the critical currents of grain boundaries in $\text{YBa}_2\text{Cu}_3\text{O}_{7-\delta}$. *Europhys. Lett.* **47**, 110–115 (1999). <https://doi.org/10.1209/epl/i1999-00359-2>
40. G. Hammerl, A. Schmehl, R.R. Schulz, B. Goetz, H. Bielefeldt, C.W. Schneider, H. Hilgenkamp, J. Mannhart, J. Mannhart, Enhanced supercurrent density in polycrystalline $\text{YBa}_2\text{Cu}_3\text{O}_{7-\sigma}$ at 77 K from calcium doping of grain boundaries. *Nature* **407**, 162–164 (2000). <https://doi.org/10.1038/35025014>
41. B.A. Malik, M.A. Malik, K. Asokan, Enhancement of the critical current density in YBCO/Ag composites. *Chin. J. Phys.* **55**, 170–175 (2017). <https://doi.org/10.1016/j.cjph.2016.10.015>

Publisher's Note Springer Nature remains neutral with regard to jurisdictional claims in published maps and institutional affiliations.